Enhanced ferroelectricity in perovskite oxysulfides

Muhammad Sheeraz,[1] Hye Jung Kim,[1] Kyou-Hyun Kim,[2] Jong-Seong Bae,[3] Ah Young Kim,[4] Manil Kang,[5] Jongmin Lee,[6] Jaesun Song,[6] Abdul Khaliq,[1] Jinkwon Kim,[7,8] Byeong-Gwan Cho,[9] Sung-Yoon Joe,[10] Jong Hoon Jung,[11] Jae-Hyeon Ko,[10] Tae Yeong Koo,[9] Tae Won Noh,[7,8] Shinuk Cho,[1] Sanghan Lee,[6] Sang Mo Yang,[4] Young-Han Shin,[1] Ill Won Kim,[1] Chang Won Ahn,[1,*] and Tae Heon Kim[1,*]

[1]Department of Physics and Energy Harvest Storage Research Center (EHSRC), University of Ulsan, Ulsan 44610, Republic of Korea
[2]Korea Institute for Rare Metal, Korea Institute of Industrial Technology, Incheon 21999, Republic of Korea
[3]Busan Center, Korea Basic Science Institute, Busan 46742, Republic of Korea
[4]Department of Physics, Sookmyung Women's University, Seoul 04310, Republic of Korea
[5]Department of Physics, Kongju National University, Kongju 32588, Republic of Korea
[6]School of Materials Science and Engineering, Gwangju Institute of Science and Technology (GIST), Gwangju 61005, Republic of Korea
[7]Center for Correlated Electron Systems, Institute for Basic Science (IBS), Seoul 08826, Republic of Korea
[8]Department of Physics and Astronomy, Seoul National University (SNU), Seoul 08826, Republic of Korea
[9]Pohang Accelerator Laboratory, POSTECH, Pohang, Gyeongbuk 790-784, Republic of Korea
[10]Department of Physics, Hallym University, Chuncheon, Gangwondo 24252, Republic of Korea
[11]Department of Physics, Inha University, Incheon 22212, Republic of Korea

(Received 28 March 2019; published 9 August 2019)

A sulfur element is a promising anion dopant for synthesizing new multifunctional materials and for exploring unusual physical phenomena. However, owing to its volatility, sulfur substitution to oxide materials is challenging, and thus the sulfurization effects on the associated properties have been limitedly studied. Here, a facile method for sulfurization to a perovskite oxide $Pb(Zr,Ti)O_3$ is developed and demonstrated. A thiourea (CH_4N_2S) solution is used as a precursor for the sulfurization and its doping-level control. By manipulating the sulfur concentration (x), we systematically examine the physical properties of sulfur-doped $Pb(Zr,Ti)O_{3-x}S_x$ films. An enhancement in the tetragonality and ferroelectricity by sulfurization is observed with the band-gap reduction, which is consistent with our theoretical predictions. In the sulfurized films, the ferroelectric phonon modes become softened progressively, probably due to the substitution of apical oxygens with sulfur atoms. Our work is of practical interest for designing ferroelectric photovoltaic devices with high performances.

DOI: 10.1103/PhysRevMaterials.3.084405

I. INTRODUCTION

Perovskite oxysulfides $ABO_{3-x}S_x$, where the apical or equatorial oxygen sites in perovskite transition-metal oxides ABO_3 are partially substituted by sulfur S atoms, are of great interest. Their fascinating physical phenomena (i.e., the enhanced ferroelectricity [1,2], the band-gap tuning [3,4], the improved photocatalytic activity [5,6], the structural phase transition [1,2], and so forth) can enable the realization of novel multifunctional devices [1–6]. Due to the isovalent nature of a sulfur S atom ($3s^2 3p^4$) with an oxygen O atom ($2s^2 2p^4$), an oxygen atom is easily substituted with a sulfur atom [2]. Note that a sulfur atom possesses a larger ionic radius (∼1.84 Å) than an oxygen atom (∼1.4 Å) [7,8]. With the substitution of the oxygen atom with the sulfur atom, the initial perovskite structure is distorted with the modification of the crystallographic symmetry and an optical gap in the electronic band structure becomes reduced with the broadening of the bandwidth [1,2]. For perovskite oxysulfide $PbTiO_{3-x}S_x$, it was theoretically reported that the polar Ti displacement with respect to the equatorial oxygen atoms is further enhanced, when the apical oxygen atom in the parent compound is replaced by a sulfur atom [1]. It was also found that the tetragonality in the sulfurized $PbTiO_{3-x}S_x$ distinctly increases resulting in higher spontaneous polarization compared with the pure $PbTiO_3$. With the enhancement in ferroelectricity and tetragonality, an indirect band gap in the electronic structure becomes narrowed from 3.44 ($PbTiO_3$) to 2.25 eV ($PbTiO_2S$) [1]. Similar behaviors by sulfurization were predicted in a tetragonal perovskite oxysulfide $KNbO_2S$, too [2].

The effect of sulfurization on physical properties in perovskite oxides has been limitedly studied due to the challenging synthesis of perovskite oxysulfides with high crystallinity [3–6,9–11]. Despite a few earlier reports of the structural, electronic, optical, photovoltaic, and photocatalytic properties in bulk perovskite oxysulfides [3,5,6,12], a systematic experimental study of the sulfurization effects has been rare. Note that most of previous theoretical results were derived from the first-principles calculations with primitive unit cells without considering possible disorder in actual experiments at finite temperatures [1,2]. Accordingly, perovskite-oxysulfide single crystals with high crystallinity are essential for a fair comparison of theoretical predictions with experimental results. Based on the previous literature, however, most of

*Corresponding authors: cwahn@ulsan.ac.kr; thkim79@ulsan.ac.kr

 ©2019 American Physical Society

the bulk perovskite-oxysulfide compounds are ceramics with polycrystallinity (i.e., the coexistence of many grains with different crystallographic orientations) [3–6]. Experimentally, it is very difficult to synthesize bulk single crystals with a sufficient amount of sulfur due to the volatility of the sulfur element [3,6,9,12,13]. In the case of the conventional solid-state-reaction method [3,6,9,12,13] a sintering process at a high temperature above 1000 °C is usually required for the crystallization [3,6,9,12,13]. Under such a high sintering temperature, sulfur atoms are readily vaporized and thereby, the overall sulfur content in the bulk compound becomes significantly deficient [3,6,9,10,12,13]. Therefore, to overcome this limitation, a new approach should be developed and then be implemented for studying the sulfurization effects on perovskite oxides systematically.

A key to realize perovskite oxysulfides with high crystallinity is to separate the sulfur-doping process from the sample fabrication. With this design strategy, various synthetic methods have been utilized for the sulfurization of complex oxides such as chemical vapor deposition (CVD) in a two-zone furnace [14,15], thermal annealing under either CS_2 [3,10] or H_2S gas flow [4,16], and so on [3,4,10,14–16]. Here, a source oxide material is first prepared and then the base material is chemically reacted with a precursor (e.g., CS_2 and H_2S) incorporating a sulfur element at a particular temperature, which produces an oxysulfide. Nevertheless, for the cases of both the CVD and thermal annealing techniques, precise control of the sulfur-doping concentration turned out to be quite difficult [3,4,10,14–16], albeit the base oxide material was sulfurized successfully. Thus, an alternative route needs to be explored for the artificial design to perovskite oxysulfides with the stoichiometric control of the sulfur content.

In this work, we have established a new and facile method to realize perovskite oxysulfides with high crystallinity. In our technique, a thiourea (CH_4N_2S) solution, where S^{2-} is able to act as a substitute for O^{2-}, is used as a precursor for sulfurization. First, a thiourea solution is spin-coated on a specimen surface and then is thermally annealed for the diffusion of sulfur atoms inside the sample. While manipulating the mole concentration of the thiourea solution, it is feasible to control the sulfur-doping level in the resulting oxysulfides quantitatively. Hence, we can systematically examine the sulfurization effects on their physical properties, which enables us to compare experimental results with theoretical calculations directly. When sulfur is doped to high-crystalline $Pb(Zr,Ti)O_3$ (PZT) films, it is experimentally identified that the ferroelectric polarization is enhanced with an increase in the tetragonality, which is in agreement with theoretical predictions. The pronounced tetragonal distortion and thereby the increase of ferroelectric transition temperature are clearly demonstrated by synchrotron x-ray diffraction analyses. It is highly likely that an apical oxygen atom is replaced by a sulfur atom leading to further softening of ferroelectric phonon modes in the PZT oxysulfides. In addition to the enhanced ferroelectricity, the reduction of a band gap is observed, which can be attributed to the bandwidth broadening by sulfur substitution. Based on the experimental observations, the potential of our sulfur-doping technique will be discussed as an aspect of multifunctional material design.

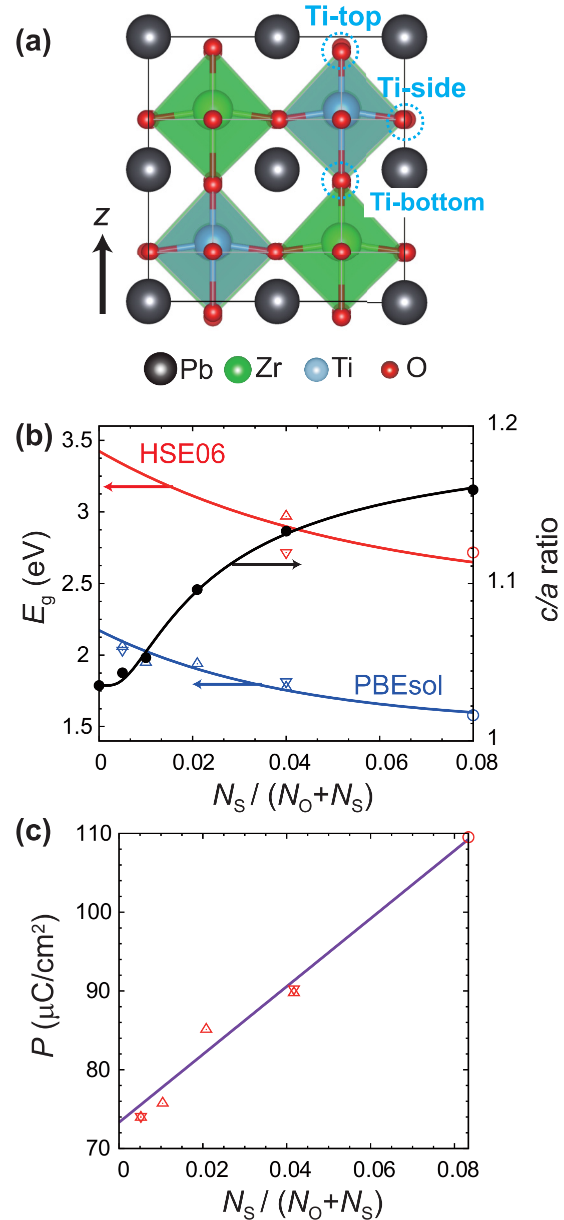

FIG. 1. Theoretical calculations of the sulfurization effect on $Pb(Zr_{0.5}Ti_{0.5})O_3$. (a) Atomic structure of tetragonal $Pb(Zr_{0.5}Ti_{0.5})O_3$ with a uniform distribution of Ti and Zr. Three distinguishable oxygen sites relative to Ti are denoted. (b) The variations of the c/a ratio and the band gap (E_g) with PBEsol and HSE06 exchange-correlation functionals. (c) The polarization P along the z direction at the sulfur substitution ratio $N_S/(N_O + N_S)$ of tetragonal $Pb(Zr_{0.5}Ti_{0.5})O_{3-x}S_x$.

II. RESULTS

A. Theoretical predictions of a sulfurization effect on $Pb(Zr_{0.5}Ti_{0.5})O_3$

The effect of sulfur doping on the structural and electrical properties in ferroelectric PZT is theoretically examined through first-principles calculations. In these calculations, we construct the tetragonal $Pb(Zr_{0.5}Ti_{0.5})O_3$ structure with a uniform distribution of Ti and Zr [space group $I4mm$ (No. 107)] as shown in Fig. 1(a) (for more details of the computational method, see the Supplemental Material [17]). A sulfur

atom is substituted for an oxygen atom in the tetragonal $Pb(Zr_{0.5}Ti_{0.5})O_3$, which has three distinguishable O sites: the Ti-top, Ti-side, and Ti-bottom sites, as marked in Fig. 1(a). Through the calculation of the formation energies for three different S-substituted PZT structures [$E_f = E(\mathrm{PZT-S}) - E(\mathrm{PZT}) + \mu(\mathrm{O}) - \mu(\mathrm{S})$, where $\mu(\mathrm{O})$ and $\mu(\mathrm{S})$ are the chemical potentials of the O and S atoms] [18], we confirm that the structure is very unstable for the replacement of the Ti-side oxygen atom with a sulfur atom ($E_f = 4.053$ eV/atom), by comparison with the other sulfur substitution cases [Ti top (3.198 eV/atom) and Ti bottom (3.795 eV/atom)]. Therefore, we only consider the effect of sulfur substitution for the Ti-top and Ti-bottom oxygen sites. Interestingly, as the sulfur substitution ratio increases, the c/a ratio (i.e., tetragonality) increases [the black solid line in Fig. 1(b)]. Due to the larger ionic radius of the sulfur atom than that of the oxygen atom, the PZT unit cells become more elongated along the c axis and the Zr and Ti ions are off-centered further. With the promoted polar displacements of Zr and Ti atoms, it is evident that ferroelectric polarization in the sulfurized PZT increases, as the sulfur concentration increases (Fig. 1(c) and Table SI of the Supplemental Material [17]). In contrast to the enhanced tetragonality and ferroelectricity, it is found that the electronic band gap decreases with the increasing sulfur concentration [Fig. 1(b)]. Note that the band gap in tetragonal PZT is determined by the O $2p$ and Ti $3d$ orbital states, which mainly contribute to the valence band maximum (VBM) and conduction band minimum (CBM), respectively. In substitution of a sulfur atom for an oxygen atom, the S $3p$ orbital states are formed at the VBM. The broadening of the S $3p$ band of the VBM is larger than increment of the energy difference between CBM and the band edge formed by O $2p$, which leads to the band-gap reduction in the electronic structure (Figs. S1 and S2 of the Supplemental Material [17]).

B. Synthesis of perovskite oxysulfides

To validate our theoretical predictions of sulfur-substituted PZT experimentally, we prepared PZT films and then sulfurized them by spin-coating a thiourea (CH_4N_2S) solution on the PZT film surface and via the successive thermal annealing for its diffusion. A high-crystalline $Pb(Zr_{0.52}Ti_{0.48})O_3$ film, which is compositionally at the morphotropic phase boundary (MPB) in the bulk compound [19–21], was first synthesized on a $SrRuO_3$ (10 nm, bottom electrode)/$SrTiO_3$ (001) heterostructure using the sol-gel method (for more information of the PZT film fabrication, see the sample-synthesis part of the Supplemental Material [17]). In the vicinity of MPB, the PZT film is structurally monoclinic and this monoclinic symmetry is very sensitive to external stimuli such as chemical doping [22], temperature [23], electric field [23–26], mechanical stress [23,27,28], and so on [22–28]. The structural sensitivity of such monoclinic PZT films to a chemical modification allows us to monitor a structural change by sulfur doping easily. Then, we sulfurized the monoclinic $Pb(Zr_{0.52}Ti_{0.48})O_3$ film by spin-coating a thiourea (CH_4N_2S) solution containing the isovalent S^{2-} ion with the O^{2-} ion, and the thiourea layer coated on the PZT surface was diffused into the PZT film via a thermal annealing process (Fig. S3 of the Supplemental Material [17]).

In our sulfurization method, precise control of the sulfur-doping level in the sulfurized PZT films is also attainable. To do this, a diluted PZT sol-gel solution was prepared by dissolving a conventional PZT solution in the equal volume of the acetic acid/2-methoxyethanol mixture solvent [29]. Then, the diluted PZT solution and thiourea powders were mixed together with various mole ratios, which produced a PZT oxysulfide [$Pb(Zr_{0.52}Ti_{0.48})O_{3-x}S_x$] sol-gel solution with a controlled sulfur mole concentration ($x = 0.01$, 0.02, 0.03, 0.04, and 0.05). Finally, the as-prepared $Pb(Zr_{0.52}Ti_{0.48})O_{3-x}S_x$ solution was spin-coated on a $SrRuO_3$(10 nm)/$SrTiO_3$(001) substrate, and then it was annealed in air at 650 °C for 30 minutes for crystallization (for detailed information, see the method part, Fig. S4, and Table SII of the Supplemental Material [17]).

C. Characterization of perovskite oxysulfides

To identify the crystallinity of our sulfurized PZT films, the high-resolution (HR) image was recorded in the zone axis of [100] as shown in Fig. 2. In the HR image, the sulfurized PZT thin film consists of a sulfur-doped PZT (∼170 nm)/$SrRuO_3$(10 nm)/$SrTiO_3$(001) film heterostructure. In addition, a clear lattice image indicates that the sulfurized thin film was well fabricated with good crystalline quality [Fig. 2(a)]. Selected area electron diffraction (SAED) pattern recorded in the proximity of the sulfurized PZT film/$SrRuO_3$ bottom interface reveals that the as-synthesized sulfur-doped PZT film is textured along the [001] crystallographic orientation with respect to the underlying $SrTiO_3$ substrate [Fig. 2(b)]. The crystallinity of our sulfur-doped PZT films was also confirmed by synchrotron x-ray diffraction (XRD) measurements (Fig. S5 of the Supplemental Material [17]). The chemical composition of the as-fabricated PZT film was also confirmed by chemical mapping with an energy-dispersive spectroscopy (EDS) detector [Figs. 2(c) and 2(g)]. The results show that both the film/electrode and the electrode/substrate interfaces are chemically sharp without any interfacial intermixing. While O is observed throughout the entire heterostructure, Pb and Ru only exist in the sulfur-doped PZT film and the $SrRuO_3$ electrode, respectively. In contrast, the evidence for S is not obvious only with the EDS results due to the low sulfur-doping level.

To verify the existence of sulfur atoms in our sulfurized PZT films, the sulfur and oxygen K-edge spectra were taken in x-ray photoelectron spectroscopy (XPS) measurements [Fig. 3]. For a pure PZT film, the O K-edge XPS responses were also monitored for comparison with the sulfur-doped PZT film. As shown in Fig. 3(a), XPS peaks of S^{2-} (161.8 eV) and S^{4+} (165.4 eV in the binding energy) valence states are evident for the sulfur-doped PZT film, whereas no S signal is measured for the pure PZT film. The presence of sulfur atoms diffused by our method is also identified from the XPS depth profile of a sulfurized PZT film grown on a Pt(111)/TiO_2/SiO_2/Si(100) substrate (Fig. S6 of the Supplemental Material [17]). By fitting the observed S K-edge curve via the Lorentzian functions, the volume fractions of S^{2-} [the red solid curve in Fig. 3(a)] and S^{4+} [the blue solid curve in

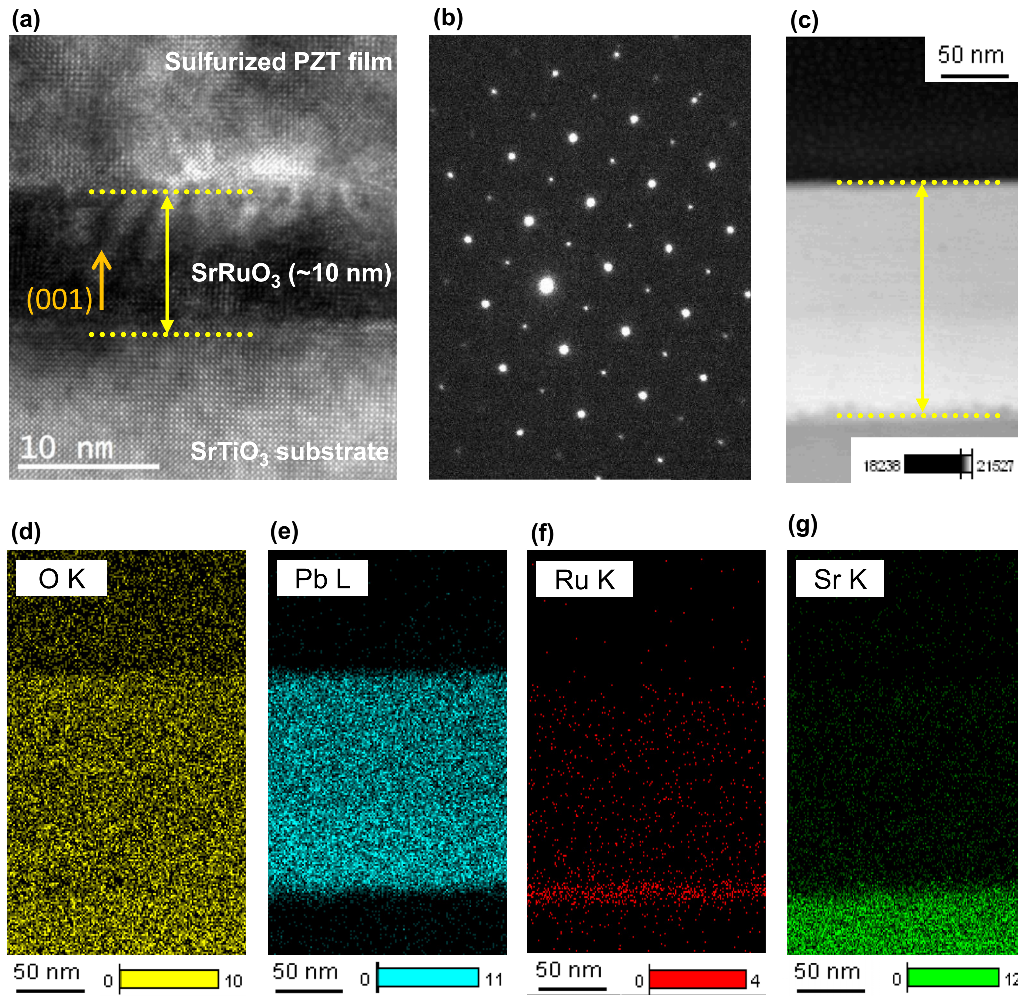

FIG. 2. Crystallinity and elemental analysis of a sulfurized $Pb(Zr_{0.52}Ti_{0.48})O_3$ film on $SrRuO_3$ (10 nm)/$SrTiO_3$ (001) substrate. (a) High-resolution transmission electron microscopy image (HRTEM) of a sulfurized PZT film grown on a $SrRuO_3/SrTiO_3$ (001) substrate (scale bar: 10 nm). (b) SAED pattern of the PZT at the interface. (c) The dotted yellow line represents the film thickness through which the composition analysis is carried out. (d)–(g) Elemental map analysis of O, Pb, Ru, and Sr, respectively.

Fig. 3(a)] states were extracted from the raw XPS data [the black solid curve in Fig. 3(a)] [30–32]. Note the S^{4+} charge valence state may arise from sulfur dioxide (SO_2) molecules on the film surface [32,33]. Since the portion (30.50%) of the S^{4+} state is much smaller than that (69.49%) of the S^{2-} state, the majority of the sulfur atoms act as an anion dopant rather than a cation dopant.

We also found that the concentration of oxygen vacancies in a PZT oxysulfide is reduced by sulfurization. As shown in the O *K*-edge XPS spectra of the pure (black solid line) and sulfurized (red solid line) PZT films [Fig. 3(a)], the XPS peak (∼531.5 eV) corresponding to oxygen vacancies is shifted towards the XPS peak (∼528.9 eV) of an oxygen atom in a perovskite oxide lattice. It has been recently reported that oxygen vacancies with a positive ionic charge are accumulated on the surface of ferroelectric films to screen negative polarization bound charges effectively [34,35]. When a ferroelectric PZT film is sulfurized, the accumulated oxygen vacancies on the film surface can be easily replaced by the provided sulfur atoms. The occupation of oxygen vacancies by sulfurization decreases the total number of oxygen vacancies leading to the lateral shift of the oxygen vacancy XPS peak. Therefore, it is highly likely that S^{2-} anions were introduced into ferroelectric PZT films through our sulfurization technique, which contributes to the reduction of oxygen vacancies as well as the substitution of the isovalent oxygen ions.

By quantifying the sulfur contents in various PZT oxysulfide films with different sulfur-doping concentrations (x) using an electron probe microanalyzer (EPMA) technique (Fig. S7 of the Supplemental Material [17]), we demonstrate that the sulfur-doping level is controllable in our sulfurization method. Evidently, the measured sulfur contents continuously increase, as the x value increases. On the contrary, oxygen content abruptly decreases for lower x (<0.02), probably due to the replacement of oxygen atoms by the sulfur dopants in our PZT oxysulfides. For higher x (>0.02), the estimated oxygen content does not keep decreasing, but rather, it becomes somewhat saturated close to the finite value.

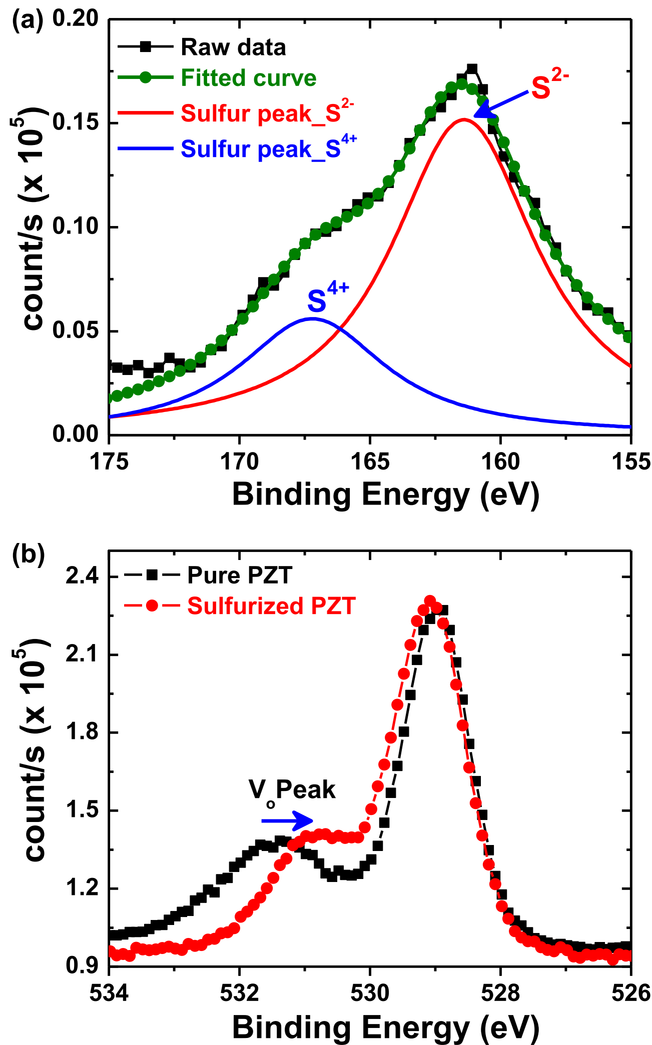

FIG. 3. X-ray photoelectron spectroscopy (XPS) measurements of a sulfurized $Pb(Zr_{0.52}Ti_{0.48})O_3$ film. (a) The S K-edge XPS spectrum of a sulfurized PZT film. The red and blue solid curves correspond to the fitting curves of the oxidation states of S^{2-} and S^{4+}, respectively. The solid red curve represents the sulfur (S^{2-}) substitution to an oxygen site, while the blue solid curve shows the presence of the SO_2 molecule on the surface of the film. (b) The O K-edge XPS spectra of pure and sulfurized PZT films.

D. Increase of tetragonality in perovskite oxysulfides

With the sulfurization of PZT films, it appears that tetragonal symmetry is predominant structurally. To examine the sulfurization effects on the crystallographic structure of our PZT/$SrRuO_3$/$SrTiO_3$ (001) films, high-resolution reciprocal space mappings (RSMs) were performed around the {103} Bragg peaks of the $SrTiO_3$ (001) substrates. For a pure $Pb(Zr_{0.52}Ti_{0.48})O_3$ film without any sulfur doping, the (103) diffraction peak of the PZT film is split along only the L direction due to structural variants by the monoclinic M_A symmetry (Fig. S8 of the Supplemental Material [17]) [36,37]. When the monoclinic PZT film is sulfurized, the peak splitting becomes weakened, and thereby, the two separated peaks become merged into a single peak indicative of a monoclinic-to-tetragonal structural transition. With the increasing sulfur-doping level from $x = 0.01$ to 0.05, the monoclinic-to-tetragonal phase transition is evident, as shown in panels (a)–(e) of Fig. 4. The L-scan profile of the $Pb(Zr_{0.52}Ti_{0.48})O_{3-x}S_x$ film peaks in Fig. 4(f) clearly shows that the two Bragg peaks induced by a monoclinic distortion become merged with a tetragonal transition, as the sulfur mole concentration increases. By plotting the in-plane (a_{PZT}) and out-of-plane (c_{PZT}) lattice constants of the sulfurized PZT films as the sulfur-doping level (x) [Fig. 4(g)], we found that c_{PZT} keeps increasing for x less than 0.03 but decreases above $x = 0.03$, whereas a_{PZT} gradually decreases with the increasing sulfur-doping concentration (x). The increase of tetragonality below the critical sulfur-doping content ($x = 0.03$) is consistent with our theoretical prediction of sulfurized PZT, but nonetheless, a further study of the decreasing tetragonality above $x = 0.03$ would be highly desirable.

E. Enhancement of ferroelectricity in perovskite oxysulfides

The tetragonal distortion by sulfurization enhances ferroelectricity in sulfur-doped PZT films. Figure 5(a) shows the polarization (P)–electric field (E) hysteresis loops of pure and sulfurized PZT (001) films. It was found that the sulfurized PZT film with larger tetragonality exhibits higher remnant polarization $[P_{avg} = (|P_+| + |P_-|)/2 = 34.3\ \mu C\ cm^{-2}]$ than the pure PZT film (22.2 μC cm^{-2}). By controlling the sulfur-doping content (x) in ferroelectric PZT films and obtaining the corresponding P-E hysteresis loops, we also found that the measured remnant polarization shows a similar tendency with the tetragonality with respect to x (Fig. S9 of the Supplemental Material [17]).

Using piezoresponse force microscopy (PFM) [Fig. 5(b)], we confirmed that the ferroelectricity of these two (i.e., pure and sulfurized) PZT films robustly exhibits strong amplitude signals [Figs. 5(b) and 5(c)] and an explicit phase contrast [Figs. 5(d) and 5(e)]. Then, the increase of ferroelectric polarization was also corroborated by comparing the magnitude of their piezoresponses relatively (Fig. S10 of the Supplemental Material [17]). For a better comparison with our theoretical predictions of enhanced ferroelectricity in PZT oxysulfides, we tested the sulfurization effect on a pure $PbTiO_3$ film with simple tetragonal symmetry (Fig. S11 of the Supplemental Material [17]). Notably, we found that the sulfur-doped $PbTiO_3$ film shows a much higher remnant polarization (26.6 μC cm^{-2}) than the pure $PbTiO_3$ film (17.9 μC cm^{-2}), which is quite consistent with our results in pure and sulfur-doped PZT films. The increments in remnant polarization of PZT (54.2%) and $PbTiO_3$ (48.2%) oxysulfides are very comparable to each other (Table SIII in the Supplemental Material [17]).

Herein, it is worthwhile to notice that a ferroelectric-to-paraelectric phase transition, which accompanies a tetragonal-to-cubic structural transition, in a sulfurized PZT film occurs at a higher Curie temperature (T_C) than the transition in a pure PZT film. For bulk $Pb(Zr_{0.52}Ti_{0.48})O_3$ (monoclinic at room temperature) at the MPB, a low-temperature ferroelectric phase (below T_C) with tetragonal symmetry is transformed to a high-temperature paraelectric phase (above T_C) with cubic symmetry at the T_C of ~640 K [19]. By carrying out the XRD θ-2θ scans of pure and sulfurized PZT films from 300 to 770 K repeatedly, we tracked how the out-of-plane lattice

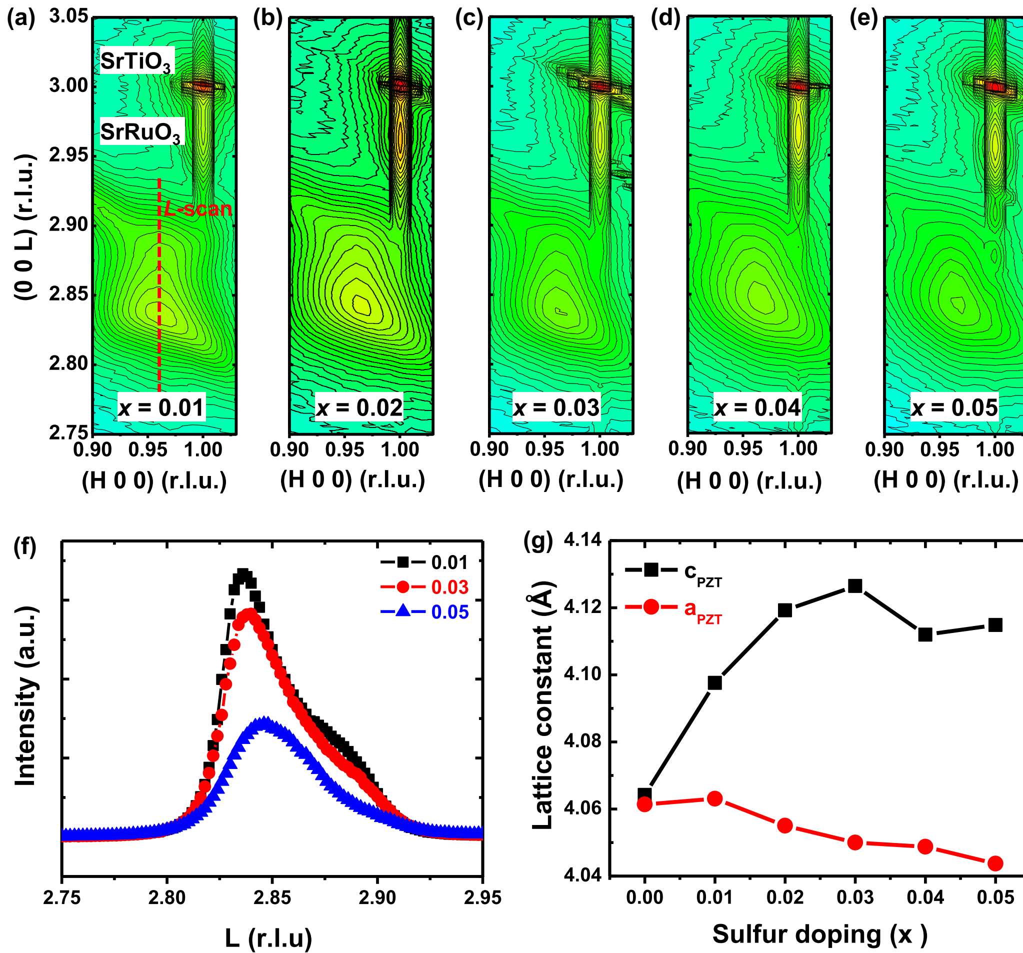

FIG. 4. The structural analyses of PZT oxysulfide [$Pb(Zr_{0.52}Ti_{0.48})O_{3-x}S_x$] films on $SrRuO_3/SrTiO_3$ substrates. (a)–(e) High-resolution RSMs of sulfur-doped PZT [$Pb(Zr_{0.52}Ti_{0.48})O_{3-x}S_x$, where $x = 0.01$, 0.02, 0.03, 0.04, and 0.05] films around the (103) Bragg peaks of $SrTiO_3$ (001) substrate. (f) The L-scan profiles [along the red dotted line in (a)] at $H = 0.96$ in the RSMs of (a)–(e). (g) The sulfur-doping level dependence of the in-plane (a_{PZT}) and out-of-plane (c_{PZT}) lattice parameters extracted from the RSM plots.

constant (c_{PZT}) evolves as a function of temperature (Fig. S12 of the Supplemental Material [17]). For the pure PZT film, it undergoes a tetragonal-to-cubic phase transition (marked by a black arrow in Fig. S12(c) of the Supplemental Material [17]) around 620 K close to T_C of bulk PZT. In contrast, two phase transitions (marked by red arrows in Fig. S12(d) of the Supplemental Material [17]) emerge in the sulfurized PZT film near 620 and 720 K. Note that the sulfur doping to a PZT film would not be uniform, because the sulfurization mainly occurs via a thermal diffusion process in our technique. Then, it is probable that the residue of unsulfurized PZT film still remains in the sulfur-doped film. It is highly likely that the transition temperatures of ~620 and 720 K originate from the phase transitions in unsulfurized and sulfurized PZT film regions, respectively. Considering the fact that a tetragonal PZT exhibits a higher T_C than a rhombohedral PZT in the bulk compound [19], the increase of tetragonality in sulfurized PZT films leads to the enhancement of the T_C.

F. Origin of enhanced ferroelectricity in perovskite oxysulfides

To elucidate the origin of the enhanced ferroelectricity in our PZT oxysulfide films, we examine the responses of ferroelectric soft-phonon modes to sulfur doping using Raman spectroscopy (Fig. 6). Note that the full Raman spectra of pure and sulfur-doped PZT films are available in Fig. S13(a) of the Supplemental Material [17] and the seven possible transverse optical (TO) phonon modes in perovskite PZT are schematically displayed in Fig. S13(b) of the Supplemental Material [17]. Among these seven TO phonon modes, only two phonon modes [i.e., horizontal $E(1TO)$ and vertical $A_1(1TO)$] are ferroelectric soft modes in PZT, where the ferroelectric polarization mostly arises from A-site Pb displacements with respect to apical oxygen atoms [38]. It is evident that the two modes are downshifted towards lower wave numbers after sulfurization [black left arrows in Fig. 6(a)]. In contrast, nonferroelectric soft modes [i.e., $E(2TO)$ and $E(3TO)$] remain unchanged from the initial wave number [red downward arrows in Figs. 6(a) and 6(b)], when a ferroelectric PZT film is sulfurized. Considering the fact that the soft phonon mode shifts are mainly activated with changes in ferroelectric properties [39], the observed peak shift in the ferroelectric Raman modes should be attributed to the increase of structural tetragonality (i.e., the elongation and shrinkage along the out-of-plane and in-plane directions, respectively) and thereby, the enhancement of ferroelectric polarization by sulfurization.

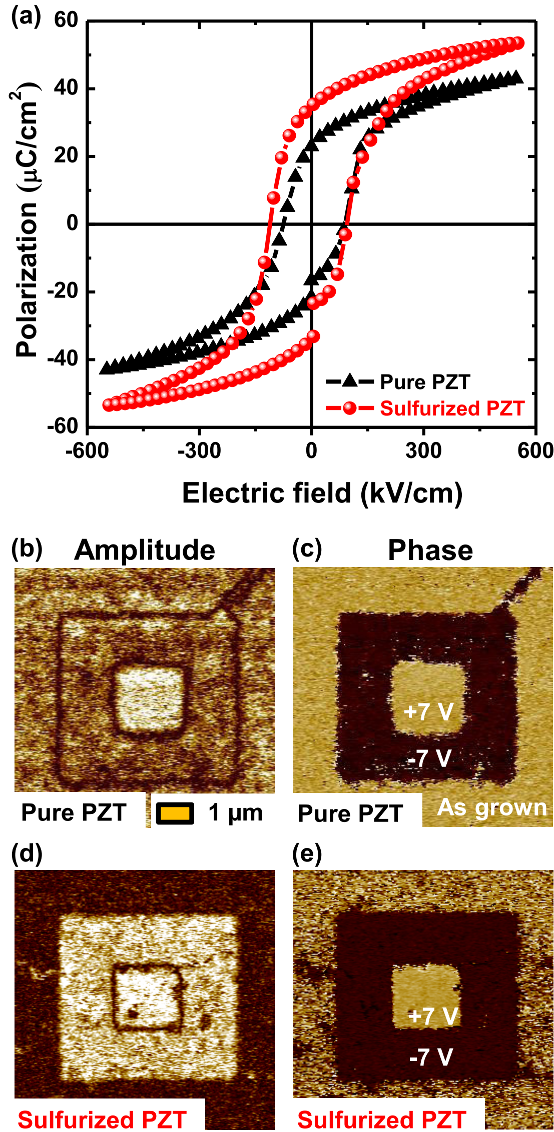

FIG. 5. Enhancement of ferroelectric polarization in sulfurized $Pb(Zr_{0.52}Ti_{0.48})O_3$ films. (a) Polarization (*P*)–electric field (*E*) hysteresis loops of pure and sulfurized PZT films on $SrRuO_3/SrTiO_3$ (001) substrate. (b)–(e) Piezoresponse force microscopy (PFM) images: (b) and (c) out-of-plane amplitude (*R*) and (d) and (e) phase (θ) mapping images of the pure and sulfurized PZT films, respectively, at the DC bias of ± 7 V.

More interestingly, another two phonon modes [i.e., A_1(2TO) and A_1(3TO)] are upshifted towards higher wave numbers after sulfurization [blue right arrows in Figs. 6(a) and 6(b)]. We note that these two phonon modes are very susceptible to the chemical bonding nature between the B-site transtion-metal *d* and the apical oxygen *p* orbitals in ABO_3 perovskite oxides (Fig. S13(b) of the Supplemental Material [17]) [40,41]. Explicitly, the frequency of A_1(2TO) and A_1(3TO) modes is described as

$$f = \frac{1}{2\pi}\sqrt{\frac{k}{m}}, \quad (1)$$

where *k* is the force constant depending on the bonding strength of the B-O hybridization [the Ti or Zr-O (S) bonding in PZT (PZT oxysulfide)] and *m* is the atomic mass of the B-site cation (Ti^{4+} or Zr^{4+} ion) [42]. Here, we stress that the Ti 3*d*–S 3*p* bonding is more covalent compared with the Ti 3*d*–O 2*p* bonding due to the lower electronegativity of the sulfur element than the oxygen atom [1]. As shown in Fig. 6(c), such strong covalency of the Ti-S (apical) bonding gives rise to a larger force constant (k_2) than the Ti-O (apical) bonding (k_1), inducing an increase in the phonon frequency, that is, an upshift in the corresponding wave number. The force constant observed from the Raman spectrum is the statistical average of the two (fluctuating Ti-S and Ti-O) bond strengths. Accordingly, it is highly plausible that an apical oxygen atom is replaced by a sulfur atom and the linked ferroelectric phonon modes are further softened in the PZT oxysulfides.

G. Reduction of the band gap in perovskite oxysulfides

In contrast with the enhancement in the tetragonality, ferroelectricity, and T_C, an electronic band gap in a sulfurized PZT film is reduced, which arises from a bandwidth expansion by the Ti 3*d*–S 3*p* covalent bonding. A decrease in the band gap was shown in the ellipsometry [Fig. 7(a)] and ultraviolet spectrometry [Fig. 7(b)] measurements of our pure and sulfurized PZT films (Fig. S14 and Table SIV of the Supplemental Material [17]). In these optical measurements, the band gaps were quantified to 3.41 and 3.32 eV for the pure and sulfurized PZT films, respectively [4,43]. And, the decrement of 0.09 eV by sulfur doping is comparable to that predicted in our theoretical calculations. The same band-gap reduction was also observed in a sulfurized PZT film with polycrystallinity (Figs. S15 and S16 and Table SV of the Supplemental Material [17]). It follows that the decrease of a band gap by sulfurization is intrinsic, that is, not attributed to an extrinsic effect (e.g., the formation of an intermediate defect level between VBM and CBM [4]). Furthermore, the reduction of the band gap also induces the increase of electrical leakage in the current density (*J*)–electric field (*E*) characteristics (Fig. S17 of the Supplemental Material [17]).

III. DISCUSSION

Despite the successful coincidence between theoretical predictions and experimental demonstrations, a discrepancy still remains. In the first-principle calculations, it was predicted that the tetragonality and ferroelectric polarization in a sulfurized PZT keep increasing, as the sulfur-doping level increases from 0.01 and 0.08 (Fig. 1). However, it was experimentally observed that the tetragonality and remnant polarization are enhanced below the lower sulfur-doping level, whereas they decrease again above the critical sulfur-doping content (Fig. 4 and Fig. S9 of the Supplemental Material [17]). Note that simple tetragonal $Pb(Zr_{0.5}Ti_{0.5})O_3$ unit cells without any disorder are assumed for the theoretical calculations of a sulfur-doping effect. Note that monoclinic $Pb(Zr_{0.52}Ti_{0.48})O_3$ films with the morphotropic chemical composition were used for the systematic investigation of the sulfurization effect on their physical properties experimentally. Structural variants by the monoclinic symmetry can induce some disorders (e.g., vacancy defects and local stress at a domain boundary) in our PZT films [36,44,45]. Such disorders impede a diffusion

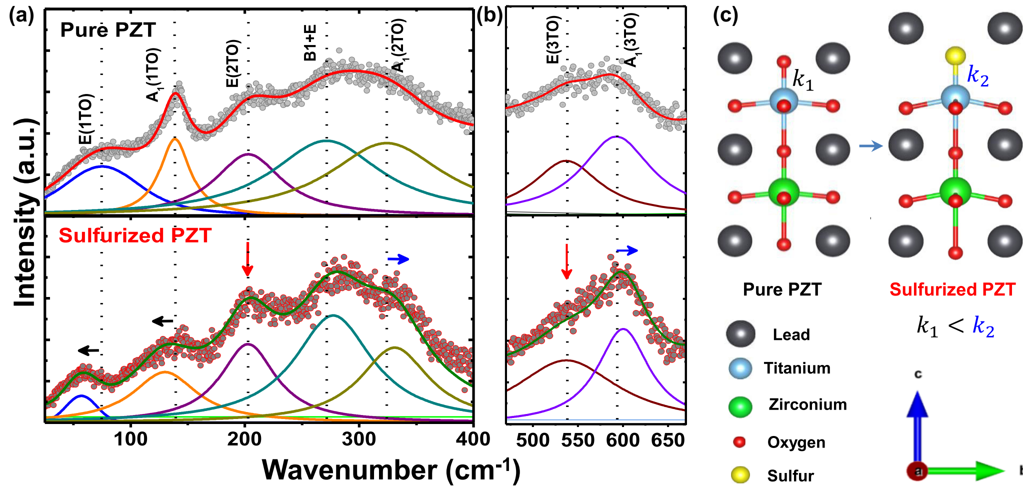

FIG. 6. The Raman spectroscopy of pure and sulfurized $Pb(Zr_{0.52}Ti_{0.48})O_3$ films. Room temperature Raman spectra of pure and sulfurized PZT films in the wave number ranges (a) 25 to 400 cm^{-1} and (b) 470 to 670 cm^{-1}. (c) Schematic demonstration of the structural transition via sulfur doping in PZT films.

process for sulfurization to take place in the whole film region uniformly, which gives rise to a nonuniform and rough sample surface in sulfurized PZT films (Fig. S18 of the Supplemental Material [17]). For better agreement between theoretical calculations and experimental observations, this limitation in the sample preparation and subsequent sulfurization should be overcome, and thus, further studies are highly desirable.

IV. SUMMARY

In summary, we developed a facile method for sulfurization to perovskite oxides and then demonstrated the sulfurization effect on their physical properties theoretically as well as experimentally. Since a thiourea (CH_4N_2S) solution is used as a precursor of the sulfurization to a target material in our technique, it is possible to control the sulfur-doping level of the synthesized oxysulfide films rather precisely. Enhancements in the structural tetragonality, the ferroelectric polarization, and the Curie temperature are attained, whereas a band gap in the electronic band structure becomes reduced. Conceptually, our work can be utilized for artificial design to new ferroelectric photovoltaic devices with high efficiency and multifunctionality.

V. METHODS

A. Theoretical calculations

We have performed our first-principles study of pure tetragonal $Pb(Zr_{0.5}Ti_{0.5})O_3$ and sulfur-substituted $Pb(Zr_{0.5}Ti_{0.5})O_3$ with a uniform distribution of zirconium (Zr) and titanium (Ti). All the calculations were computed using the Vienna *ab initio* Simulation Package (VASP) [46] based on density functional theory (DFT). The projected augmented wave method [47], the PBEsol exchange-correlation functional [48], and a kind of generalized gradient approximation (GGA) were used to optimize the structure of the sulfur-substituted $Pb(Zr_{0.5}Ti_{0.5})O_3$ [47,48]. In these calculations, we used an 800 eV cutoff energy and the atomic positions were relaxed with the conjugated gradient method until each atom force was smaller than 0.001 eV/Å. The cell volume relaxation was also performed. To examine the effect of sulfur-substituted density, we considered one or two sulfur substitutions in $2\times2\times2$, $2\sqrt{2}\times2\sqrt{2}\times2$, $2\sqrt{2}\times2\sqrt{2}\times4$, and $4\times4\times4$ $Pb(Zr_{0.5}Ti_{0.5})O_3$ supercells. For the two sulfur substitution case, the second sulfur site was determined far away from the first sulfur-substituted site. The first Brillouin zone was divided by a $4\times4\times4$ k-point mesh for the $2\times2\times2$ supercell. The k-point mesh was properly controlled according to the cell size. The hybrid functional (HSE06) was also used to obtain the more accurate band-gap values of the sulfur-substituted $Pb(Zr_{0.5}Ti_{0.5})O_3$ at higher sulfur substitution densities. The Berry phase calculations are used to achieve the spontaneous polarizations of the tetragonal $Pb(Zr_{0.5}Ti_{0.5})O_3$ and sulfur-substituted $Pb(Zr_{0.5}Ti_{0.5})O_3$.

B. Ferroelectric $Pb(Zr_{0.52}Ti_{0.48})O_3$ film fabrication

To fabricate ferroelectric $Pb(Zr_{0.52}Ti_{0.48})O_3$ (PZT) thin films with high crystallinity, we first prepared a PZT sol-gel solution (with 0.2 moles liter^{-1}) by diluting the pristine PZT (0.4 moles liter^{-1}) solution in equal volume ratio to the acetic acid/2-methoxyethanol mixture solvent. To grow a pure PZT film, we spin-coated the diluted PZT sol-gel solution on a $SrRuO_3$ (10 nm)/$SrTiO_3$ (001) film (3000 rpm for 30 s), cured the spin-coated PZT solution on a hot plate (450 °C for 7 min), and annealed in a box furnace (650 °C for 3 min). These three steps of spin coating, curing, and thermal annealing were repeated four times to deposit a PZT film with a thickness of about 170 nm (Fig. S19 of the Supplemental Material [17]). For the crystallization, we finally annealed the as-deposited PZT film at 650 °C in the box furnace for 30 min.

C. Method A: Sulfurization of perovskite $Pb(Zr_{0.52}Ti_{0.48})O_3$ films

To synthesize a sulfurized PZT thin film with high crystallinity (Fig. S3 of the Supplemental Material [17]), a pure PZT thin film was first fabricated using the sol-gel method.

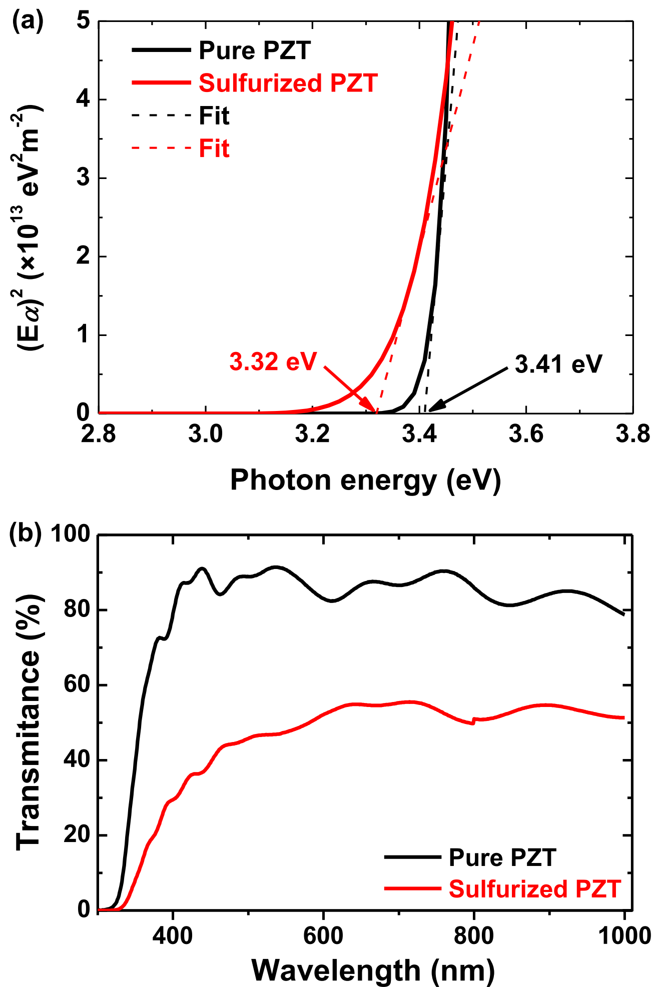

FIG. 7. The electronic band-gap measurements of pure and sulfurized $Pb(Zr_{0.52}Ti_{0.48})O_3$ films. (a) The band-gap measurement of pure and sulfurized PZT films on $SrRuO_3/SrTiO_3$ (001) substrates using ellipsometry. Here, $(E\alpha)^2$, where E and α are the photon energy and the absorption coefficient, respectively, was plotted as a function of the photon energy (eV). (b) Ultraviolet-visible spectrometry of pure and sulfurized PZT films on fluorine-doped tin oxide (FTO) coated glass substrates.

For the sulfurization of the as-fabricated PZT film, we prepared a thiourea (CH_4N_2S) solution as a precursor by dissolving thiourea powder into a mixed solvent consisting of ethanol (8 ml) and water (2 ml). Then, it was continuously stirred for 24 hr. The thiourea solution was spin-coated on the pure PZT surface (3000 rpm for 30 s), the thiourea-coated PZT film was cured on a hot plate (450 °C for 7 min), and it was annealed in a box furnace for crystallization (650 °C for 33 min). During the last thermal annealing process, sulfur ions in the surface thiourea layer were diffused inside the PZT film.

D. Method B: Precise control of the sulfur-doping level in perovskite oxysulfides

To control the sulfur-doping concentration in perovskite oxysulfide $Pb(Zr_{0.52}Ti_{0.48})O_{3-x}S_x$ thin films precisely (Fig. S4 of the Supplemental Material [17]), we first prepared a diluted PZT solution (0.2 moles liter^{-1}) by dissolving a commercial PZT solution in the equal volume of the acetic acid/2-methoxyethanol mixture solvent. The thiourea powder with various mole concentrations ($x = 0.01$, 0.02, 0.03, 0.04, 0.05) was added to the diluted PZT solution, and we kept stirring the thiourea-dissolved PZT solution for 24 hr continuously. Then, the oxysulfide solution was spin-coated on a $SrRuO_3$ (10 nm)/$SrTiO_3$ (001) film (3000 rpm for 30 s), the spin-coated oxysulfide layer was cured on a hot plate (450 °C for 7 min), and it was annealed in a box furnace (650 °C for 3 min). As done in the fabrication of pure PZT films, these three steps of spin coating, curing, and thermal annealing were repeated four times to deposit a PZT oxysulfide film with a particular thickness. For the crystallization, we also annealed the as-deposited PZT oxysulfide film at 650 °C in the box furnace for 30 min.

E. Transmission electron microscopy measurements and analyses

The crystallinities of pure and sulfurized PZT films grown on $SrRuO_3$ (10 nm)/$SrTiO_3$ (001) substrate were investigated by using high-resolution transmission electron microscopy (HRTEM) analyses. Selected-area electron diffraction (SAED) was also recorded in the zone axis of [100]. The chemical analysis and mapping at the nanometer level were performed via energy-dispersive x-ray spectroscopy (EDX). In detail, the cross-sectional samples were prepared for TEM observations. The PZT thin films were cut along the growth direction of [001] and mechanically polished down to about $\sim$15 μm. For the electron transparency, the mechanically thinned sample was further Ar-ion milled (Gatan Precision Ion Polishing System, PIPS II, Gatan, USA). Microstructural investigation was further carried out using transmission electron microscopy (TEM, TECNAI F20 S-TWIN, FEI, Netherlands) to identify the film structure. In TEM measurements, the sulfurized PZT film was fabricated using method A (Fig. 2).

F. X-ray photoelectron spectroscopy measurements and analyses

X-ray photoelectron spectroscopy (XPS) was conducted using a K-Alpha$^+$ XPS system (Thermo Fisher Scientific, Inc., UK) equipped with a monochromated Al $K\alpha$ x-ray source ($h\nu = 1486.6$ eV) of spot size 400 μm, and charge compensation of the XPS samples was performed during analysis. The carbon C 1s peak of hydrocarbon at a binding energy of 284.6 eV was used as a reference to take corrections of all the obtained spectra. The pure and sulfurized PZT films for XPS analyses were synthesized using method A (Fig. 3 and Fig. S6).

G. Synchrotron x-ray diffraction measurements

Synchrotron x-ray diffraction (XRD) experiments were performed with the 3A beamline of Pohang Accelerator Laboratory (PAL). In the XRD measurements, a 6-circle x-ray goniometer was used for the XRD θ-2θ scans and the reciprocal space mappings (RSMs) of pure and sulfurized PZT films. To obtain the in-plane and out-of-plane lattice constants of the pure and sulfur-doped PZT films, we carried out RSMs around the (103) Bragg peak of the $SrTiO_3$ (001) substrate. From

the RSM measurements, a monoclinic-to-tetragonal structural transition was visualized with the increasing sulfur-doping concentration. To measure the Curie (T_C) temperature of the pure and sulfurized PZT films, XRD θ-2θ scans around the (002) Bragg peak of the $SrTiO_3$ (001) substrate were also performed in a wide range of temperature from 300 to 770 K. By monitoring the temperature dependence of out-of-plane lattice constants in the pure and sulfurized PZT films, we extracted the T_C of a ferroelectric-to-paraelectric phase transition. We fabricated the pure and sulfurized PZT films for the room-temperature XRD analyses (Fig. S5) and the temperature-dependent XRD measurements (Fig. S12) via method A. The PZT oxysulfide films with the controlled concentration of sulfur dopants were prepared with method B for the room-temperature RSMs (Fig. 4).

H. Ferroelectric hysteresis measurements

The polarization (P)–electric field (E) hysteresis loops were obtained at room temperature using a ferroelectric tester (PRECISON LC Material Analyzer, Radiant Technologies, USA) by applying a triangular electric pulse with an amplitude of 10 V and a frequency of 1 kHz to a ferroelectric capacitor. For ferroelectric hysteresis measurements, Pt top electrodes with a diameter of 90 μm were deposited on pure and sulfurized PZT films using the direct current (DC) sputtering machine (Cressington 108, Cressington, Inc., USA). The deposition of the Pt electrodes was performed at the pressure rate of 0.06 mbar under the argon environment. To investigate the sulfurization effect on ferroelectricity, we prepared the pure and sulfurized PZT films for the P-E hysteresis measurements via method A [Fig. 5(a)]. To examine the sulfur-doping-level dependence of ferroelectric hysteresis loops, we fabricated the PZT oxysulfide films with the controlled concentration of sulfur dopants via method B (Fig. S9).

I. Piezoresponse force microscopy measurements

An atomic force microscopy (AFM) machine (NX-10: Park system) with the point probe plus electrostatic force microscopy (PPP-EFM) nanosensors tip was used for piezoresponse force microscopy (PFM). The amplitudes and phase components of the as-grown pure and sulfurized PZT films were taken by applying DC bias of ± 7 V through a conductive tip. The pure and sulfurized PZT films for PFM measurements were fabricated with method A [Fig. 5(b) and Fig. S10].

J. Ellipsometry measurements and analyses

The elliptic constants (Ψ and Δ) of the pure and sulfurized PZT films were measured using a spectroscopic ellipsometer (SE, Horiba-Jobin Yvon, Uvisel UV/NIR) with a photon energy range of 0.75 to 4.5 eV at an incident angle of 70°. SE data were analyzed by using the double new amorphous (DNA) dispersion formula with two oscillators (Fig. S14 and Fig. S15 of the Supplemental Material [17]). The pure and sulfurized PZT films for the ellipsometry analyses were prepared with method A [Fig. 7(a) and Fig. S16].

K. Raman spectroscopy

Room-temperature Raman spectroscopy of pure and sulfurized PZT films was performed at a wavelength of 532 nm by using a conventional Raman spectrometer (LabRam HR800, Horiba Co.). An optical microscope (BX41, Olympus) was used for measuring the spectrum at the backscattering geometry. The power of the laser was set to be about 40 mW. The setup combined with a supernotch filter allowed us to measure Raman spectra in the 10–1200 cm^{-1} range. Diffraction grating for the UV–NIR range was set at 1800 lines/mm. We synthesized the pure and sulfurized PZT films for the Raman measurement using method A (Fig. 6 and Fig. S13).

L. Optical transmittance measurements

Transmittance spectra of the pure and sulfurized PZT films were obtained using a high-resolution dual-beam ultraviolet-visible spectrometer (Varian, Cary 5000) with excellent photometric performance between 175 and 3300 nm. For our PZT samples, their optical transmittances were measured ranging from 300 to 1000 nm. To detect the transmittance signals, the pure and sulfurized PZT films were deposited on fluorine-doped tin oxide (FTO) coated glass substrates. It appeared that the sulfurized PZT film exhibited a lower transmittance than the pure PZT film with the increase of the transmittance-edge wavelength. This indicates that an optical band gap in the PZT film is narrowed by sulfurization. We fabricated the pure and sulfurized PZT films for the optical transmittance measurement using method A [Fig. 6(b)].

ACKNOWLEDGMENTS

T.H.K. acknowledges National Research Foundation of Korea (NRF) grants funded by the Korea government (Ministry of Education) (Grants No. 2017R1D1A1B03028614 and No. NRF-2019R1A6A1A11053838) and support by the National Research Foundation of Korea (Grant No. NRF-2014R1A4A1071686). C.W.A. acknowledges support by the Basic Science Research Program through the National Research Foundation of Korea (NRF) funded the Ministry of Science and ICT (Grant No. NRF-2018R1A2B6009210). H.J.K. acknowledges a National Research Foundation of Korea (NRF) grant funded by the Korea government (Ministry of Education) (Grant No. NRF-2017R1D1A1B03030356). S.M.Y. was supported by a National Research Foundation of Korea (NRF) grant funded by the Korean Government (MSIP) (Grant No. NRF-2017R1C1B2010258). J.H.K. acknowledges a National Research Foundation of Korea (NRF) grant funded by the Korea government (Ministry of Education) (Grant No. 2016R1A2B4012646). J.K. and T.W.N. were supported by the Research Center Program of IBS (Institute for Basic Science) in Korea (Grant No. IBSR009-D1). This research was supported by the Creative Materials Discovery Program (Grant No. 2017M3D1A1040828) through the National Research Foundation of Korea (NRF) funded by the Ministry of Science and ICT. Experiments at PLS-II were supported in part by MSICT and POSTECH.

[1] J. A. Brehm, H. Takenaka, C. W. Lee, I. Grinberg, J. W. Bennett, M. R. Schoenberg, and A. M. Rappe, Phys. Rev. B **89**, 195202 (2014).
[2] G. Amarsanaa, D. Odkhuu, C. W. Ahn, and I. W. Kim, J. Appl. Phys. **116**, 194105 (2014).
[3] S. Pereraa, H. Hui, C. Zhao, H. Xue, F. Sun, C. Deng, N. Gross, C. Milleville, X. Xu, D. F. Watson, B. Weinstein, Y.-Y. Sun, S. Zhang, and H. Zeng, Nano Energy **22**, 129 (2016).
[4] S. M. Lee and Y. S. Cho, Dalton Trans. **45**, 5598 (2016).
[5] F.-F. Li, D.-R. Liu, G.-M. Gao, B. Xue, and Y.-S. Jiang, Appl. Catal. B **166–167**, 104 (2015).
[6] A. Ishikawa, Y. Yamada, T. Takata, J. N. Kondo, M. Hara, H. Kobayashi, and K. Domen, Chem. Mater. **15**, 4442 (2003).
[7] R. D. Shannon and C. T. Prewitt, Acta Cryst. B **25**, 925 (1969).
[8] R. D. Shannon, Acta Cryst. A. **32**, 751 (1976).
[9] S. Niu, H. Huyan, Y. Liu, M. Yeung, K. Ye, L. Blankemeier, T. Orvis, D. Sarkar, D. J. Singh, R. Kapadia, and J. Ravichandran, Adv. Mater. **29**, 1604733 (2017).
[10] A. Clearfield, Acta Cryst. **16**, 135 (1963).
[11] Y. Wang, N. Sato, and T. Fujino, J. Alloys Compd. **327**, 104 (2001).
[12] M. Itoh and Y. Inabe, Phys. Rev. B **68**, 035107 (2003).
[13] B. Okai, K. Takahashi, M. Saeki, and J. Yoshimoto, Mater. Res. Bull. **23**, 1575 (1988).
[14] I. Bilgin, F. Liu, A. Vargas, A. Winchester, M. K. L. Man, M. Upmanyu, K. M. Dani, G. Gupta, S. Talapatra, A. D. Mohite, and S. Kar, ACS Nano **9**, 8822 (2015).
[15] J. Ma, K. Tang, H. Mao, J. Ye, S. Zhu, Z. Xu, Z. Yao, S. Gu, and Y. Zheng, Appl. Surf. Sci. **435**, 297 (2018).
[16] R. Lelieveld and D. Ijdo, Acta Cryst. B **36**, 2223 (1980).
[17] See Supplemental Material at http://link.aps.org/supplemental/10.1103/PhysRevMaterials.3.084405 for more details on theoretical calculations, experimental procedure, XRD spectra, EPMA analysis, RSM measurement, PFM measurements, electrical analyses, Raman spectroscopy, and band-gap calculations.
[18] S. B. Zhang and J. E. Northrup, Phys. Rev. Lett. **67**, 2339 (1991).
[19] B. Noheda, J. A. Gonzalo, L. E. Cross, R. Guo, S. E. Park, D. E. Cox, and G. Shirane, Phys. Rev. B **61**, 8687 (2000).
[20] B. Noheda, D. E. Cox, G. Shirane, J. Gao, and Z.-G. Ye, Phys. Rev. B **66**, 054104 (2002).
[21] B. Noheda, D. E. Cox, G. Shirane, J. A. Gonzalo, L. E. Cross, and S.-E. Park, Appl. Phys. Lett. **74**, 2059 (1999).
[22] C. S. Tu, V. H. Schmidt, I. C. Shih, and R. Chien, Phys. Rev. B **67**, 020102(R) (2003).
[23] M. Davis, D. Damjanovic, and N. Setter, Phys. Rev. B **73**, 014115 (2006).
[24] F. Bai, N. Wang, J. Li, and D. Viehland, J. Appl. Phys. **96**, 1620 (2004).
[25] B. Noheda, Z. Zhong, D. E. Cox, G. Shirane, S.-E. Park, and P. Rehrig, Phys. Rev. B **65**, 224101 (2002).
[26] R. Chien, V. H. Schmidt, C.-S. Tu, L.-W. Hung, and H. Luo, Phys. Rev. B **69**, 172101 (2004).
[27] Z. Chen, Z. Luo, C. Huang, Y. Qi, P. Yang, L. You, C. Hu, T. Wu, J. Wang, C. Gao, T. Sritharan, and L. Chen, Adv. Funct. Mater. **21**, 133 (2011).
[28] H. M. Christen, J. H. Nam, H. S. Kim, A. J. Hatt, and N. A. Spaldin, Phys. Rev. B **83**, 144107 (2011).
[29] Y. J. Ko, D. Y. Kim, S. S. Won, C. W. Ahn, I. W. Kim, A. I. Kingon, S.-H. Kim, J.-H. Ko, and J. H. Jung, ACS Appl. Mater. Interfaces **8**, 6504 (2016).
[30] X. Tang and D. Li, J. Phys. Chem. C **112**, 5405 (2008).
[31] D. Gonbeau, C. Guimon, G. Pfister-Guillouzo, A. Levasseur, G. Meunier, and R. Dormoy, Surf. Sci. **254**, 81 (1991).
[32] D. I. Sayago, P. Serrano, O. Böhme, A. Goldoni, G. Paolucci, E. Román, and J. A. Martin-Gago, Phys. Rev. B **64**, 205402 (2001).
[33] T. Umebayashi, T. Yamaki, H. Itoh, and K. Asai, Appl. Phys. Lett. **81**, 454 (2002).
[34] M. F. Chisholm, W. Luo, M. P. Oxley, S. T. Pantelides, and H. N. Lee, Phys. Rev. Lett. **105**, 197602 (2010).
[35] D. Lee, S. H. Baek, T. H. Kim, J.-G. Yoon, C. M. Folkman, C. B. Eom, and T. W. Noh, Phys. Rev. B **84**, 125305 (2011).
[36] B. H. W. Jang, D. Ortiz, S.-H. Baek, C. M. Folkman, R. R. Das, P. Shafer, Y. Chen, C. T. Nelson, X. Pan, R. Ramesh, and C.-B. Eom, Adv. Mater. **21**, 817 (2009).
[37] B. Y.-H. Chu, M. P. Cruz, C.-H. Yang, L. W. Martin, P.-L. Yang, J.-X. Zhang, K. Lee, P. Yu, L.-Q. Chen, and R. Ramesh, Adv. Mater. **19**, 2662 (2007).
[38] G. Burns and B. A. Scott, Phys. Rev. Lett. **25**, 167 (1970).
[39] D. A. Tenne, P. Turner, J. D. Schmidt, M. Biegalski, Y. L. Li, L. Q. Chen, A. Soukiassian, S. Trolier-McKinstry, D. G. Schlom, X. X. Xi, D. D. Fong, P. H. Fuoss, J. A. Eastman, G. B. Stephenson, C. Thompson, and S. K. Streiffer, Phys. Rev. Lett. **103**, 177601 (2009).
[40] J. D. Freire and R. S. Katiyar, Phys. Rev. B **37**, 2074 (1988).
[41] M. K. Zhu, P.-X. Lu, Y.-D. Hou, X. M. Song, H. Wang, and H. Yan, J. Am. Ceram. Soc. **89**, 3739 (2006).
[42] D. Fu, T. Ohno, T. Ogawa, H. Suzuki, K. Ishikawa, and T. Hayashi, Jpn. J. Appl. Phys. **39**, 5687 (2000).
[43] X. Yang, X. Su, M. Shen, F. Zheng, Y. Xin, L. Zhang, M. Hua, Y. Chen, and V. G. Harris, Adv. Mater. **24**, 1202 (2012).
[44] M. W. Chu, I. Szafraniak, R. Scholz, C. Harnagea, D. Hesse, M. Alexe, and U. Gosele, Nat. Mater. **3**, 87 (2004).
[45] V. Nagarajan, A. Roytburd, A. Stanishevsky, S. Prasertchoung, T. Zhao, L. Chen, J. Melngailis, O. Auciello, and R. Ramesh, Nat. Mater. **2**, 43 (2003).
[46] G. Kresse and J. Furthmuller, Phys. Rev. B **54**, 11169 (1996).
[47] P. E. Blochl, Phys. Rev. B **50**, 17953 (1994).
[48] J. P. Perdew, A. Ruzsinszky, G. I. Csonka, O. A. Vydrov, G. E. Scuseria, L. A. Constantin, X. Zhou, and K. Burke, Phys. Rev. Lett. **100**, 136406 (2008).